separation into a reticulate part able to capture air bubbles when partly submerged, and a smooth hydrophilic part to stand on, it is impossible to sustain a large portion of the egg well above the surface of a liquid larval food.

We thank Prof. Dr. Vera Lucia Imperatriz Fonseca for providing the bees, and Prof. Dr. Carminda da Cruz Landim for providing the neutral red stain. Mr. Gerard Stooker (Utrecht), and Mr. Eduardo T. Matos (São Paulo) provided substantial technical assistance, for which we express our gratitude. Financial support was given by FAPESP.

1. Michener CD (1974) The social behavior of the bees. Belknap, Cambridge
2. Sakagami SF (1982) Stingless bees. In: Hermann RH (ed) Social insects, vol III. Academic, New York, pp 361–423
3. Michener CD, Grimaldi D (1988) The oldest fossil bee: Apoid history, evolutionary stasis, and antiquity of social behaviour. Proc Natl Acad Sci USA 85:6424–6426
4. Hartfelder KH, Engels W (1989) The composition of larval food in stingless bess: evaluating nutritional balance by chemosystematic methods. Insectes Sociaux 36:1–14
5. Camargo CA de (1976) Dieta semi-artificial para abelhas da subfamília. Meliponinae (Hymenoptera, Apidae). Ciência e Cultura 28:430–431
6. Sommeijer MJ, van Zeijl M, Dohmen MR (1984) Morphological differences between worker-laid eggs from a queenright colony and a queenless colony of *Melipona rufiventris paraensis* (Hymenoptera: Apidae). Entomol Ber Amsterdam 44:91–95
7. Koedam D (1995) Behavioural and physiological implications of queen dominance in stingless bees. Thesis, University of Utrecht
8. Koedam D, Velthausz PH, van der Krift T, Dohmen MR, Sommeijer MJ (1996) Morphology of reproductive and trophic worker eggs and their controlled release by workers in *Tetragonisca angustula* (Apidae, Meliponinae). Physiol Entomol 21:289–296
9. Benthem FDJ van, Imperatriz Fonseca VL, Velthuis HHW (1995) Biology of the stingless bee *Plebeia remota* (Holmberg): observations and evolutionary implications. Insectes Sociaux 42:71–87
10. Drumond PM, Zucchi R, Mateus S, Bego L (1996) Oviposition behavior of the stingles bees, XVII. *Plebeia (Plebeia) droryana* and an ethological comparison with other Meliponine taxa (Hymenoptera, Apidae). Jpn J Entomol 64:385–400
11. Beig D (1972) The production of males in queenright colonies of *Trigona (Scaptotrigona) postica.* J Apicultural Res 11:33–39

Naturwissenschaften 85, 333–339 (1998) Springer-Verlag 1998

Polarization Portrait of the Arago Point: Video-polarimetric Imaging of the Neutral Points of Skylight Polarization

Gábor Horváth, József Gál, István Pomozi
Department of Biological Physics, Eötvös University, H-1088 Budapest, Puskin u. 5-7, Hungary, e-mail: gh@hercules.elte.hu

Rüdiger Wehner
Zoologisches Institut, Universität Zürich, CH-8057 Zurich, Winterthurerstrasse 190, Switzerland, e-mail: rwehner@zool.unizh.ch

Received: 29 December 1997 / Accepted in revised form: 8 April 1998

In 1809 the French astronomer Dominique Francois Jean Arago discovered the polarization of skylight [1]. Soon thereafter he observed a point of zero polarization in the sky [1], which nowadays is called the Arago neutral point. About 30 years later the French meteorologist Jacques Babinet found a second neutral point in the celestial hemisphere [2], and a few years later a third one was discovered by the Scottish physicist Sir David Brewster [3]. These neutral points have been the subject of many investigations in both the 19th and the 20th centuries [4–11]. In spite of their scientific popularity in atmospheric optics [5–11], until now they have not been able to be imaged due to the lack of proper wide-field polarimeters. We report here on the first polarization portrait of the Arago neutral point. In our video-polarimetric imaging study the spatial distribution of the degree and angle of polarization of the Arago point is presented in the red, green, and blue spectral ranges.

The most important optical characteristics of the clear sunlit sky are well described by Rayleigh's theory [11]. The fine details of skylight polarization, however, differ from the ideal Rayleigh model. This failure, called the polarization defect, is caused by multiple scattering, molecular anisotropy, multi-order scattering by aerosol particles, size distribution and particle shapes of aerosol, and the light reflected from the ground. One of the most remarkable features of this defect is the phenomenon of the neutral points, where the polarization vanishes.

Under normal clear atmospheric conditions, the only neutral points of skylight polarization are the Arago [1], Babinet [2], and Brewster [3] points located in the plane of the sun's vertical (Fig. 1). These neutral points have been observed much more than any other characteristic of the skylight po-

Correspondence to: G. Horváth

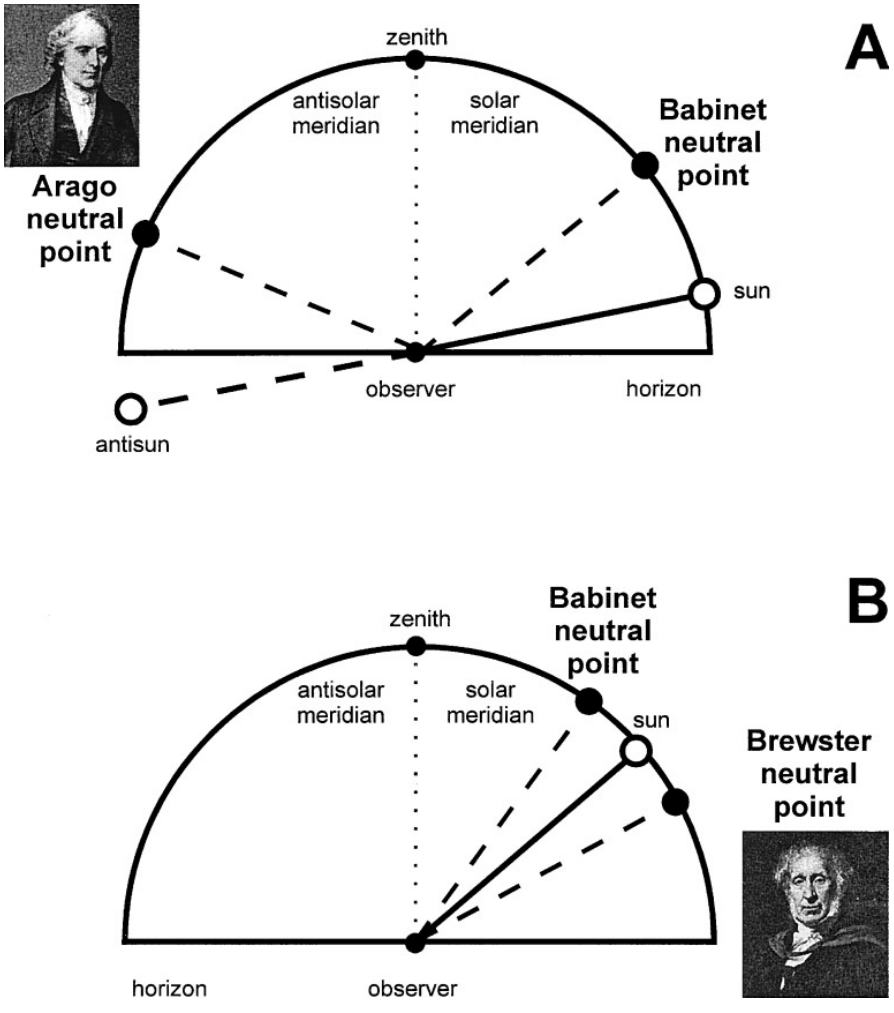

Fig. 1A,B. Schematic diagram showing the normal positions of the Arago, Babinet, and Brewster neutral points of skylight polarization in the plane of the sun's vertical. *Insets*, the portraits of Dominique Francois Jean Arago (1786–1853) and Sir David Brewster (1781–1868), the discoverer of the first and third neutral points, respectively

larization. Van de Hulst [6] gave an approximate derivation for the angular position of the neutral points, which vary with solar altitude, wavelength, and haze aerosol composition. Neuberger [5] suggested that systematic observation of the Arago point would provide an appropriate index of atmospheric turbidity. Sekera [7], Holzworth and Rao [8], and Bellver [10] found a reasonably good correlation between positions of the neutral points and the intensity of air pollution. The positions of the neutral points are also strongly modified by clouds and debris from large volcanic eruptions, even for periods of several years [11].

For a neutral point to occur in the sky, the normally positive polarization of skylight – in which the maximum of the electric field vector (E-vector, or major axis of the polarization ellipse of light) is normal to the plane of scattering; the latter passes through the observer, the sun, and the point observed – must be matched exactly by an equal quantity of negative polarization – in which the E-vector is oriented parallel to the plane of scattering. Multiple scattering of light causes negative polarization [4]. The stronger the multiple scattering, the more negative polarization is introduced in the atmosphere, and the more the neutral points are displaced from their position computed for primary scattering. The amount of multiple scattering is strongly affected by atmospheric turbidity.

According to Coulson [11], the Arago point is located 20–30° above the antisolar point, called the "antisun" (the point at the celestial hemisphere that lies opposite the sun; Fig. 1A). Its location in the portions of the sky opposite to the sun renders it the easiest one to be observed. This is the reason why the Arago point has been observed more frequently than either of the other two neutral points. The Babinet point is located 25–30° above the sun (Fig. 1). This position makes it observable any time the sun is above the horizon, and for considerable periods of time before sunrise and after sunset. Being closer to the sun, and hence in a brighter part of the sky than the Arago point, the Babinet point is somewhat less readily seen than the Arago point. The Brewster point is located 25–30° below the sun (Fig. 1B). The region between the sun and the horizon is the brightest area of the sky, and haze near the horizon yields generally low polarization values, so that the Brewster point is very difficult to observe. Under normal atmospheric conditions, only two – either the Arago and the Babinet point (Fig. 1A) or the Babinet and the Brewster point (Fig. 1B) – are visible at any one time. The Babinet and Brewster points move closer to the sun as the sun rises higher in the sky. They merge into a single neutral point coincident with the sun when the sun reaches the zenith.

In spite of the fact that the neutral points have been characterized by measurements performed with both visual and electronic instruments, until now they could not be visualized due to the lack of proper imaging devices (imaging polarized light analysers). Most ground-based observations of the neutral points have been performed visually by means of the Savart polariscope [11]. This simple device was widely used for more than a century, and still has not been entirely supplanted by electronic polarimeters. The neutral points can be detected, and their position can accurately be determined by using the Savart polariscope. However, this po-

lariscope is not well suited for determining the degree of polarization. Modern electronic polarimeters use narrow-band interference filters to determine the position of the neutral points for different wavelengths. As they possess a very small aperture (diameter ca. 1–4°), polarization characteristics can be analyzed only within a very restricted field of view. Of course, the spatial distribution of the degree and angle (orientation) of polarization at and around the neutral points could be determined by scanning the respective areas with such polarimeters, but this is a troublesome and time-consuming task which can be accomplished only in the laboratory by complicated, computer-aided procedures. Therefore it is not surprising that so far no one has studied the neutral points using this technique.

In the atmospheric sciences most polarimeters are used in connection with photomultipliers as detecting devices. The need for polarized images in remote sensing led first to the use of photographic films, then to the use of television tubes, and most recently to that of video-cameras as detectors. Walraven [12] discussed general methods of analysing of polarized photographic images. Wehner [13] took wide-field images of the sky by using a 180° fish-eye lens equipped with a linear polarizer to portray celestial E-vector patterns for various elevations of the sun, as did Können [9] in his work on polarized light in nature. Most recently Wehner [14] presented a photographic image of the entire celestial hemisphere using a set of 22 circumferentially polarizing filters (so-called axis finders), which were mounted on a transparent plexiglas dome. An exploratory program for obtaining photographs taken through a linearly polarizing filter from the Space Shuttle has been carried out by Coulson et al. [15]. Most recently North and Duggin [16] developed a practical method for obtaining partial Stokes vectors and derivative images of the celestial hemisphere by taking advantage of a four-lens photographic camera.

Prosch et al. [17] used a video-polarimeter for observations of the Earth's surface from an aircraft. Egan [18] designed an imaging polarimeter for satellite application. Recently several authors used wide-field or video-polarimetry for different measurements in computer vision [19], in remote sensing of clouds from satellite [20], and in biological studies [21–25]. In spite of the rapid development of video polarimeters and their convenient applicability in the atmospheric sciences, until now neither of the neutral points of skylight polarization had been imaged using these recently available devices.

To fill this gap we recorded the spatial distributions (patterns) of the degree and the angle (direction) of polarization within the areas of the neutral points using video-polarimetry, which is described in detail elsewhere (see [24]). We did so by first filming the selected region of the sky with a video-camera recorder (CCD-VX1E Sony video Hi8 Handycam) through a linearly polarizing filter (Hama, mounted dichroic sheet neutral grey polarizer) in front of the objective lens. The camera was set up on a tripod. Pitch angle, focus, aperture, shutter speed, and gain were adjusted manually, and any automatic correction or adjustement of the camera electronics was switched off. During recording, the polarizer was turned stepwise in 45° intervals. The initial orientation of the transmission axis of the filter was vertical. After a few seconds the filter was turned twice by 45°; thus its final orientation was horizontal. The orientation of the filter was recorded as an audio-signal by a built-in microphone.

Afterwards the recorded scenes were digitized frame by frame using a frame grabber (Screen Machine II, Fast Multimedia, Munich) in a personal computer (Pentium) connected to a stop-frame video recorder (Sony EV-C500E Hi8). For all three orientations, $\varphi = 0°$, 45°, and 90°, of the polarizer 25 digitized frames were averaged to filter the inevitable small noise of the video signal. From these three averaged video-pictures we obtained the modulation of the brightness (intensity) I as a function of φ. A sinusoid ($I = A \sin \varphi + B$) was fitted to this brightness modulation for each pixel of the picture, to determine I_{max}, I_{min}, and the angular position χ of I_{max}. From these parameters we calculated the total light intensity, $I = (I_{max} + I_{min})/2$, and the degree of polarization, $\delta = (I_{max} - I_{min})/(I_{max} + I_{min})$, for every point in the image. Finally, we produced a two-dimensional false-colour map of the brightness I, degree of polarization δ, and E-vector alignment χ on the computer screen. With our camcorder the maximal field of view was 50° in the horizontal and 40° in the vertical direction. Using the CCD-VX1E video-camera recorder we could process all polarized-light information in three colour channels, red (R, $\lambda_{red} = 730 \pm 65$ nm), green (G, $\lambda_{green} = 600 \pm 65$ nm) and blue (B, $\lambda_{blue} = 470 \pm 65$ nm). This procedure resulted in 3×3 pictures of any particular skylight area of which we took records: The patterns of brightness, degree and direction of polarization were recorded in the R, G, and B spectral ranges.

The neutral points were recorded under clear sky conditions on 8 August 1996 in the vicinity of Metlaoui in the mountainous area of central Tunisia. This site and time was ideal for the recordings because the atmosphere was very clear, exhibiting a minimal amount of haze and aerosol. As a consequence the degree of polarization was high enough to allow any video-polarimetric imaging of the neutral points. For the sake of simplicity the polarization patterns are presented here only for the most famous and popular neutral point, the Arago point. The recordings were made at sunset (19:15 hours local time; pitch angle of camera 20°). The Babinet and Brewster points were also imaged by the same procedures as described above. As their polarization characteristics are nearly identical with those of the Arago point, we refrain from presenting them here.

Figure 2A represents a colour picture of the sky in the region of the Arago point. The backscattered reddish glow of the setting sun near the horizon (demarcated by a reddish brown mountain ridge) and the blue of the sky above the rising antisun are clearly visible. It is obvious from Fig. 2A–D that the polarization-blind human eye is not able at all to perceive any neutral point because the posi-

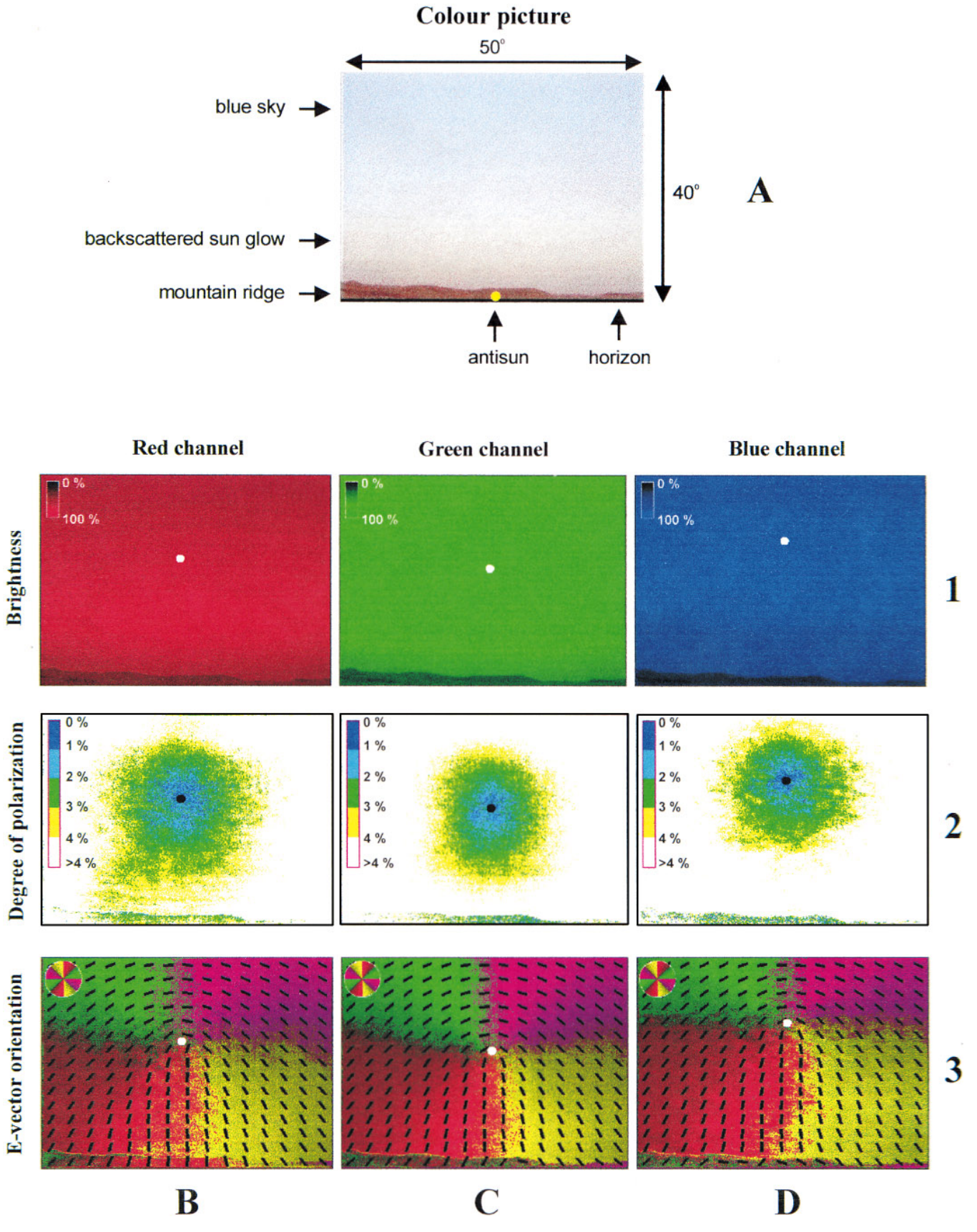

Fig. 2A–D. Video-polarimetric imaging of the Arago neutral point of skylight polarization. A) Colour picture of the sky around the Arago point as obtained by video-recording. The horizontal and vertical angular extension of the scene is 50° and 40°, respectively. *Yellow dot*, position of the antisun. The horizon is demarcated by a reddish brown mountain ridge. B)–D) The patterns of brightness (intensity) I (*row 1*), degree of polarization δ (*row 2*) and E-vector orientation (angle of polarization) χ (*row 3*) of the sky measured by video-polarimetry in the *red* (column B, $\lambda_{red} = 730 \pm 65$ nm), *green* (column C, $\lambda_{green} = 600 \pm 65$ nm), and *blue* (column D, $\lambda_{blue} = 470 \pm 65$ nm) channels. The different numerical values of I, δ, and χ are encoded in the different shades of colour: (a) the higher the light intensity, the brighter the red, green and blue shade of colour (black, I = 0%; brightest, I = 100%); (b) dark blue: $0\% \le \delta < 1\%$, light blue: $1\% \le \delta < 2\%$, green: $2\% \le \delta < 3\%$, yellow: $3\% \le \delta < 4\%$, white: $\delta > 4\%$; (c) the darker the violet/green and the red/yellow shade of colour, the stronger the deviation of the orientation of the E-vector from the horizontal and vertical, respectively (*red*: $0° \le \chi < 45°$; *green*: $45° \le \chi < 90°$; *violet*: $90° \le \chi < 135°$; *yellow*: $135° \le \chi \le 180°$). *Row 3*, *any particular black bar* represents the local orientation of the E-vector as averaged over a small rectangular region around the bar. The positions of the Arago point are indicated by *white dots* (*rows 1, 3*) and *black dots* (*row 2*)

tions of the neutral points are not correlated with the brightness and colour in the sky. In contrast, the Arago point is clearly visible in the pictures portraying the degree of polarization (row 2 in Fig. 2) and the angle of polarization (E-vector orientation; row 3 in Fig. 2). As it is clearly demonstrated in row 2 of Fig. 2, skylight is unpolarized (d = 0%) in the centre of the neutral point; the degree of polarization gradually increases with increasing angular distance from this centre.

The patterns of the E-vector alignment in row 3 of Fig. 2 show that the direction of polarization is more or less vertical (shaded with red and yellow colours), that is, the polarization is negative between the Arago point and the antisun, but above the Arago point the E-vectors are more or less horizontal (shaded with green and violet colours), indicating positive polarization. Furthermore, as can be seen in the patterns of E-vector orientation, polarization switches from negative to positive as one passes the neutral point parallel to the antisolar meridian.

The histograms of Fig. 3 present the distribution of the orientation and degree of polarization as calculated for the celestial region at and around the Arago point imaged in Fig. 2. Row 1 in Fig. 3 demonstrates well that the regions of positive and negative polarization are symmetrically arranged around the Arago point. Row 2 of the same figures shows that around the Arago point the degree of polarization is very low (smaller than 14–15%).

There is one additional result to mention. The different angular positions of the Arago point in the red, green, and blue ranges of the spectrum (see Fig. 2) demonstrate well the polarization dispersion in the sky. Under normal atmospheric conditions a general rule is that the shorter the wavelength of light, the lower the degree of polarization [11]. There is little spectral dependency at the longer wavelength range ($\lambda > 500$ nm), but very strong dispersion for shorter wavelengths. The strong variation of the degree of polarization at shorter wavelengths is due mainly to multiple scattering because the degree of polarization resulting from a single scattering event is essentially independent of wavelength. At shorter wavelengths multiple scattering reduces the degree of polarization, increasing the magnitude of negative polarization and thus shifting the positions of the neutral points. The region of negative polarization surrounding the sun and antisun is much more extended in the short-wavelength (ultraviolet and blue) than the long-wavelength (green and red) range of the spectrum. This is the reason why usually the angular distances of the neutral points from the antisun and sun increase as the wavelength of light decreases [11]. Consequently in the visible range of the spectrum the Arago point is placed nearest the horizon in the red spectral range. In the green range it is positioned a slightly farer away from the horizon, and in the blue its angular distance from the horizon is the greatest.

Rows 2 and 3 of Fig. 2 clearly show that the Arago point is farest away from the antisun in the blue range of the spectrum. The measured angular distance β of the Arago point from the antisun is $\beta_{red} = 24.4°$, $\beta_{green} = 22.4°$, $\beta_{blue} = 29.3°$ in the red, green, and blue ranges, respectively. Hence at the time of our video-polarimetric recordings the Arago point was slightly closer to the antisun in the green spectral range than in the red one. This exceptional situation was caused by the ground reflection of light.

Reflection from rough-surface ground introduces more or less vertically polarized light into the atmosphere. This effect enhances the region of negative polarization of the sky in those spectral ranges in which the reflectivity of the ground is high. At the site of our video-polarimetric measurements in the vicinity of Metlaoui in central Tunisia the soil and the mountains had a typical reddish brown colour (see the bottom of Fig. 1A). Thus the ground reflection (albedo) was high in the red spectral range. The consequence was that in the red range of the spectrum a considerable amount of vertically polarized light was reflected from the ground, which enhanced the contribution of negative polarization in the atmosphere. Thus the Arago point shifted slightly farer away from the antisun in the red range.

A similar shift of the position of the Arago point due to reflection from snow or bright sand has also been reported by other authors [9, 11]. In such cases, however, the shift of the Arago point was observed in all ranges of the spectrum because the ground reflection was high in all spectral ranges due to the whiteness of snow or sand. Reflection of light from huge water surfaces (lakes or sea) affects the position of the Arago point in the opposite direction. Light reflected from water surfaces introduces horizontally polarized light into the atmosphere in all spectral ranges, which enhances the region of positive polarization. This effect results in a shift of the Arago point towards the antisun in every range of the spectrum [9, 11].

According to Coulson [11], more attention has been paid to the measure-

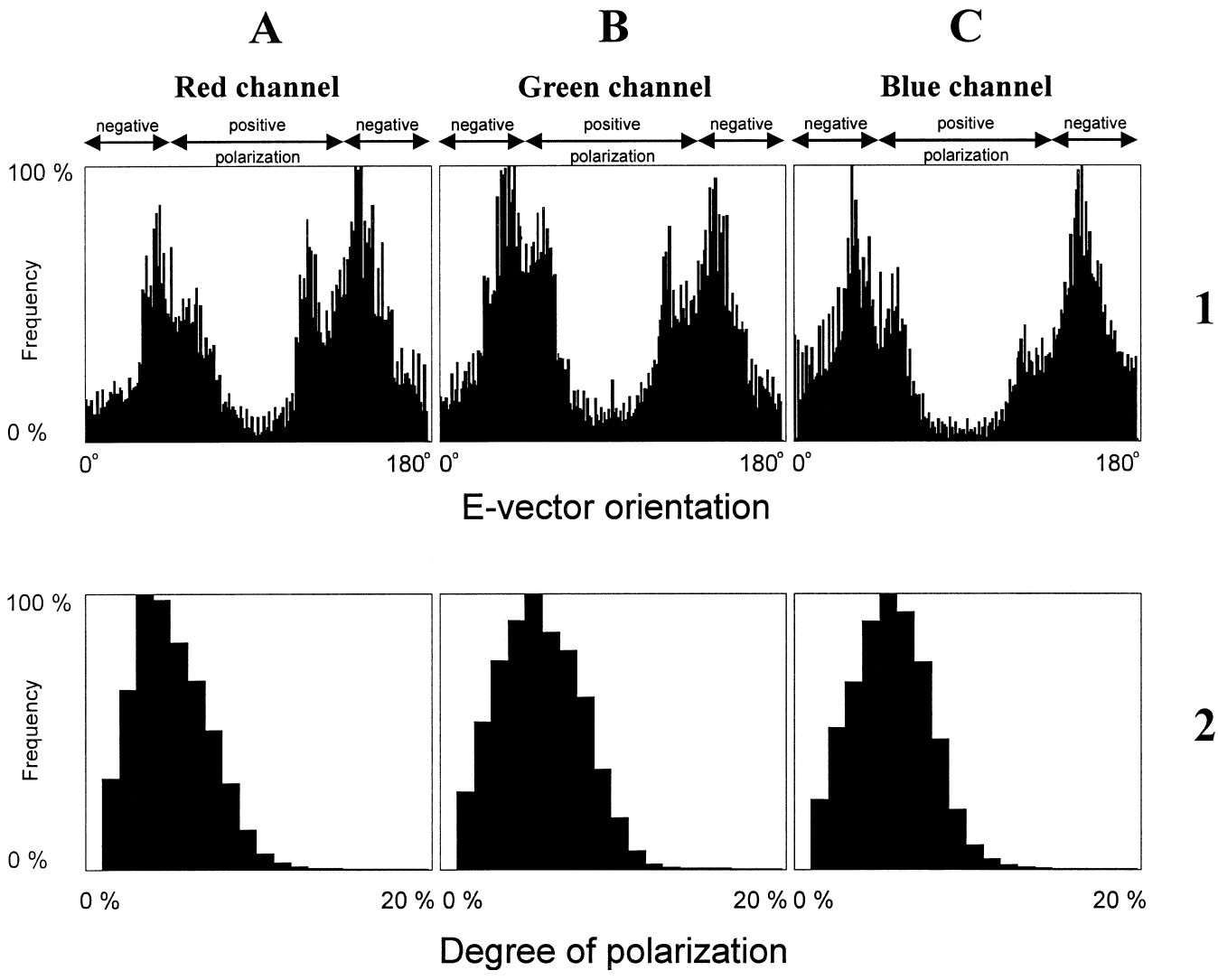

Fig. 3. Frequency distributions of E-vector orientation (*row 1*) and degree of polarization (*row 2*) in the red (*column A*), green (*column B*), and blue (*column C*) ranges of the spectrum. All data refer to the region of the sky at and around the Arago neutral point imaged in Fig. 2

ment of neutral point positions than to any other feature of skylight polarization. These studies are now complemented by our direct visualization of the neutral points and their surrounding skylight areas. The novelty of this approach consists in the polarization imaging of the neutral-point areas of the sky, and the presentation of high-resolution false-colour maps of the degree and orientation of polarization within these areas.

In conclusion, the polarization pictures in Fig. 2 and the histograms in Fig. 3 portray the main characteristics of the neutral points: (a) their angular distances from the antisun and sun, (b) how their distances vary as a function of the wavelength of light, (c) how ground reflection affects their position, (d) what regions of positive and negative polarization occur around these points, and (e) that there is no correlation between the positions of the neutral points and the brightness and colour distributions in the sky.

The work was supported by grant OTKA F-014923 received from the Hungarian National Science Foundation (G.H.) and grant 31-43317.95 of the Swiss National Science Foundation (R.W.). The critical comments of Ákos Horváth (University of Arizona, Institute of Atmospheric Physics, Tucson) and of two anonymous referees are gratefully acknowledged. Many thanks are due to our colleague Dr. Viktor Horváth for his help in the digitization of the video records.

1. Barral MJA (1858) Oeuvres de Francois Arago I–V. Gide, Paris; Weigel, Leipzig
2. Babinet J (1840) Sur un nouveau point neutre dans l'atmosphere. Comptes Rendus 11:618–620
3. Brewster D (1847) On the polarisation of the atmosphere. Phil Mag J Sci 31:444–454
4. Chandrasekhar S (1950) Radiative Transfer. Clarendon, Oxford

5. Neuberger H (1950) Arago's neutral point: a neglected tool in meteorological research. Bull Am Met Soc 31:119–125
6. Van de Hulst HC (1952) Scattering in atmospheres. In: Kniper GP (ed) The atmosphere of the earth and planets. University of Chicago Press, Chicago
7. Sekera Z (1957) Light scattering in the atmosphere and the polarization of skylight. J Opt Soc Am 47:484–490
8. Holzworth GC, Rao CR (1965) Studies of skylight polarization. J Opt Soc Am 55:403–408
9. Können GP (1985) Polarized light in nature. Cambridge University Press, Cambridge
10. Bellver C (1987) Influence of particulate pollution on the positions of neutral points in the sky at Seville (Spain). Atmospheric Environment 21:699–702
11. Coulson KL (1988) Polarization and intensity of light in the atmosphere. Deepak, Hampton
12. Walraven RL (1981) Polarization imagery. Opt Eng 20:14–18
13. Wehner R (1976) Polarized-light navigation by insects. Sci Am 235(1):106–114
14. Wehner R (1997) The ant's celestial compass system: spectral and polarization channels. In: Lehrer M (ed) Orientation and communication in arthropods. Birkhäuser, Basel, pp 145–185
15. Coulson KL, Whitehead VS, Campbell C (1986) Polarized views of the earth from orbital altitude. Proc SPIE 637, Ocean Optics VIII:35–41
16. North JA, Duggin MJ (1997) Stokes vector imaging of the polarized sky-dome. Appl Opt 36:723–730
17. Prosch T, Hennings D, Raschke E (1983) Video polarimetry: a new imaging technique in atmospheric science. Appl Opt 22:1360–1363
18. Egan WG (1986) Proposed design of an imaging spectropolarimeter/photometer for remote sensing of earth resources. Opt Eng 25:1155–1159
19. Wolff LB (1993) Polarization camera technology. Proc DARPA Image Understanding Works, pp 1031–1036
20. Deschamps PY, Bréon FM, Leroy M, Podaire A, Bricaud A, Buriez J C, Séze G (1994) The Polder mission: instrument characteristics and scientific objectives. IEEE Trans Geosci Rem Sens 32:598–615
21. Cronin TW, Shashar N, Wolff LB (1994) Portable imaging polarimeters. Proc 12th IAPR Int Conf Pattern Recogn, pp 606–609
22. Shashar N, Cronin TW, Johnson G, Wolff LB (1995) Portable imaging polarized light analyzer. SPIE Proc series 2426:28–35
23. Horváth G, Zeil J (1996) Kuwait oil lakes as insect traps. Nature 379:303–304
24. Horváth G, Varjú D (1997) Polarization pattern of freshwater habitats recorded by video polarimetry in red, green and blue spectral ranges and its relevance for water detection by aquatic insects. J Exp Biol 200:1155–1163
25. Horváth G, Gál J, Wehner R (1997) Why are water-seeking insects not attracted by mirages? The polarization pattern of mirages. Naturwissenschaften 84:300–303

Naturwissenschaften 85, 339–342 (1998) Springer-Verlag 1998

Novel and Highly Specific Transport of a Volatile Sex Pheromone by Hemolymph Lipophorin in Moths

Coby Schal, Veeresh Sevala
Department of Entomology, North Carolina State University, Box 7613, Raleigh, NC 27695-7613, USA

Ring T. Cardé
Department of Entomology 041, University of California, Riverside, CA 92521, USA

Received: 22 December 1997 / Accepted in revised form: 16 April 1998

Here we report that in *Holomelina* tiger moths (Lepidoptera: Arctiidae) pheromone is synthesized by tissues associated with the abdominal integument, and that lipophorin, a multifunctional plasma lipoprotein, transports the pheromone to an abdominal gland that stores and releases the pheromone only during active calling behavior. We suggest that such transport pathways are common not only among insects that emit hydrocarbon pheromones but also among insects that sequester hydrophobic plant-derived metabolites.

Animals have evolved sophisticated chemical communication systems, including volatile sex pheromones that are used in mate recruitment, and cuticular constituents that elicit courtship and copulation upon contact (Cardé and Minks 1997). In most insects sex pheromones are produced in and emitted from specialized pheromone glands, and in female moths these glands generally constitute an epidermal layer near the female's ovipositor (Percy-Cunningham and MacDonald 1987). These glands synthesize de novo all the components of the pheromone blend (Bjostad et al. 1987; Jurenka and Roelofs 1993), and although mechanisms of pheromone export to the exterior remain unknown, these lipophilic compounds presumably require little if any interaction with an aqueous environment.

Species within the genus *Holomelina* emit pheromone blends of normal and 2-methyl-branched alkanes ranging in chain length from 16 to 19 carbons. The main pheromone component of several species is 2-methylheptadecane (2Me-17:Hy) which attracts males in field assays (Roelofs and Cardé 1971; Schal and Cardé 1985). In *H. lamae*, as in other arctiids, the pheromone emanates from paired tubular glands that vent between the 8th and 9th abdominal segments (Yin et al. 1991). Two independent observations led us to test the hypothesis that pheromone is not syn-

Correspondence to: C. Schal